

Towards Generalizable Robotic Manipulation in Dynamic Environments

Heng Fang¹, Shangru Li¹, Shuhan Wang¹, Xuanyang Xi²,
Dingkang Liang^{1†}, and Xiang Bai¹

¹ Huazhong University of Science and Technology

² Huawei Technologies Co. Ltd

[†]Project Lead.

{hengfang,dkliang}@hust.edu.cn

Abstract. Vision-Language-Action (VLA) models excel in static manipulation but struggle in dynamic environments with moving targets. This performance gap primarily stems from a scarcity of dynamic manipulation datasets and the reliance of mainstream VLAs on single-frame observations, restricting their spatiotemporal reasoning capabilities. To address this, we introduce **DOMINO**, a large-scale dataset and benchmark for generalizable dynamic manipulation, featuring 35 tasks with hierarchical complexities, over 110K expert trajectories, and a multi-dimensional evaluation suite. Through comprehensive experiments, we systematically evaluate existing VLAs on dynamic tasks, explore effective training strategies for dynamic awareness, and validate the generalizability of dynamic data. Furthermore, we propose **PUMA**, a dynamics-aware VLA architecture. By integrating scene-centric historical optical flow and specialized world queries to implicitly forecast object-centric future states, PUMA couples history-aware perception with short-horizon prediction. Results demonstrate that PUMA achieves state-of-the-art performance, yielding a 6.3% absolute improvement in success rate over baselines. Moreover, we show that training on dynamic data fosters robust spatiotemporal representations that transfer to static tasks. All code and data are available at <https://github.com/H-EmbodVis/DOMINO>.

Keywords: Dynamic Manipulation · Vision-Language-Action Model · Embodied AI

1 Introduction

Recent advancements in Vision-Language-Action (VLA) models have demonstrated significant success in handling manipulation tasks, establishing a foundation for generalizable embodied intelligence [3, 13, 47, 52]. However, most existing VLA models [4, 5, 24, 25] focus on static manipulation, which involves interacting with stationary objects in stable environments. In contrast, dynamic manipulation requires robots to adapt to moving objects and continuous environmental changes. Mastering this capability is essential for deploying robots in complex real-world scenarios, such as operating on active assembly lines or working alongside humans. Despite its importance, dynamic manipulation remains a critical

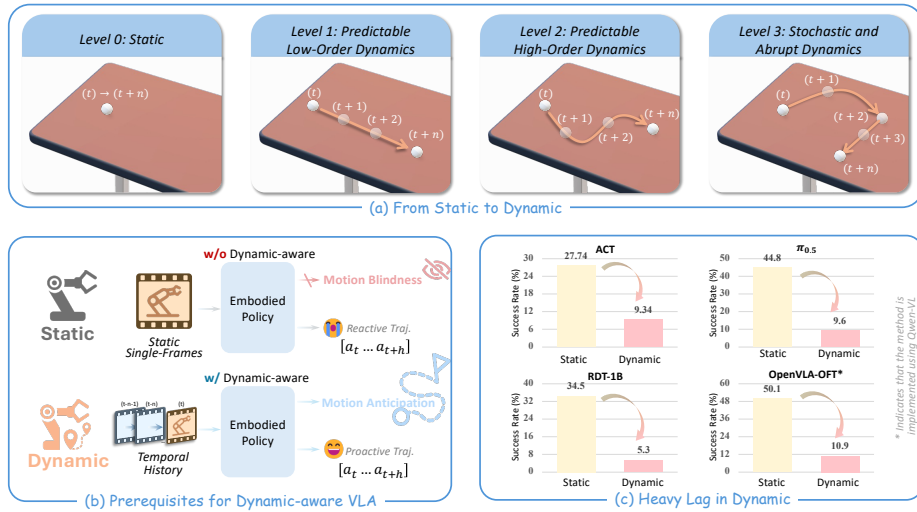


Fig. 1: (a) Illustration of the defined dynamic difficulty levels, progressing from static (Level 0) to stochastic and abrupt dynamics (Level 3). (b) Dynamic awareness requires capturing historical context and anticipating future motion. (c) Performance of SOTA models degrades when shifting from static to dynamic environments.

yet underexplored frontier. Dynamic manipulation is inherently difficult as it imposes strict requirements on spatiotemporal precision and necessitates the continuous integration of real-time perception with motion prediction. Progress in this domain is hindered by two primary factors: **1)** the scarcity of large-scale dynamic manipulation datasets, and **2)** the limited dynamic perception and motion prediction capabilities of existing mainstream VLA architectures.

High-quality dynamic data is indispensable for achieving generalizable dynamic manipulation. Addressing the current data scarcity is non-trivial due to the inherent complexity of dynamic tasks. Constructing dynamic environments for data collection presents significant challenges, primarily due to the strict spatiotemporal synchronization required between moving targets and robotic actions. Furthermore, acquiring expert demonstrations in such unpredictable settings is difficult, as human teleoperators or scripted policies often struggle to react precisely to continuous environmental changes. Consequently, most existing embodied datasets are confined to stationary tasks [6, 38, 51]. Therefore, developing a scalable, low-cost pipeline to acquire diverse manipulation data in dynamic scenarios is a critical imperative.

To bridge this gap, we introduce a comprehensive benchmark tailored for generalizable dynamic manipulation, termed the **Dynamic Object Manipulation Operations Benchmark (DOMINO)**. Building upon RoboTwin 2.0 [10] and the SAPIEN [55] simulation engine, we develop scalable pipelines for dynamic manipulation dataset generation and closed-loop evaluation. The benchmark comprises 35 diverse dynamic tasks across 5 distinct robot embodiments, spanning from single-arm operations to complex dual-arm collaborations. As shown in Fig. 1(a), these tasks are organized into a three-tiered difficulty hierarchy, progress-

ing from predictable low-order dynamics to high-order nonlinear trajectories and stochastic scenarios with abrupt disturbances. To precisely control task complexity, we parameterize the overall motion speed using a scalar dynamics coefficient α , denoting each setting as *DOMINO@ α* . Crucially, these tasks present significant challenges for current VLA models. While existing VLAs excel at static manipulation, they struggle in dynamic environments due to an inherent lack of continuous spatiotemporal reasoning. The precise timing required to interact with moving targets and handle unexpected disturbances often exceeds the capabilities of current architectures, which are typically constrained by static spatial biases. To rigorously assess generalization, our dataset provides over 110K expert trajectories collected under both canonical and domain-randomized settings. Finally, our closed-loop pipeline establishes a multi-dimensional evaluation protocol that extends beyond standard binary success rates.

Evaluations of state-of-the-art models [5, 25, 32, 63] on this benchmark reveal substantial performance degradation in dynamic settings, as shown in Fig. 1(b). We attribute this decline to the reliance of standard VLA architectures on single-frame observations, which limits their dynamic awareness. We suggest that this awareness requires *capturing historical context and anticipating future motion*. Although recent VLAs incorporate world models [9, 57, 61], they primarily model global scene transitions or robot kinematics, neglecting the individual object dynamics crucial for spatiotemporal anticipation. To address this, we present PUMA as an exploratory attempt to bridge this gap. By integrating historical frames and motion cues to model scene-centric historical dynamics, our method introduces specialized predictive queries to implicitly infer object-centric dynamics for moving targets. This design endows the model with a dynamic understanding of the physical world, enabling anticipatory interactions with moving objects and yielding a 6.3% SR improvement.

In summary, the main contributions are as follows: **1)** We systematically analyze dynamic manipulation, distinguishing its unique spatiotemporal challenges from static paradigms to underscore the need for advancing dynamic embodied intelligence. **2)** We introduce DOMINO, a scalable pipeline for dynamic manipulation dataset generation and closed-loop evaluation. It features diverse robot embodiments, multi-tiered difficulty scaling via a dynamics coefficient, and a comprehensive four-dimensional metric suite. **3)** We propose PUMA, which integrates historical motion cues to enhance motion anticipation. By employing specialized predictive queries to implicitly infer the future states of moving objects, our approach yields a 6.3% performance improvement over baselines.

2 DOMINO Dataset

2.1 Task Definition

We formulate generalizable dynamic manipulation as a Partially Observable Markov Decision Process (POMDP) [22]. At time step t , the full state $s_t = \{s_t^r, s_t^o\}$ comprises the robot proprioception s_t^r and the physical object state s_t^o . Due to partial observability, the policy relies on an observation history $o_{t-h:t}$, where each observation $o_t = \{I_t, s_t^r\}$ includes high-dimensional visual inputs I_t

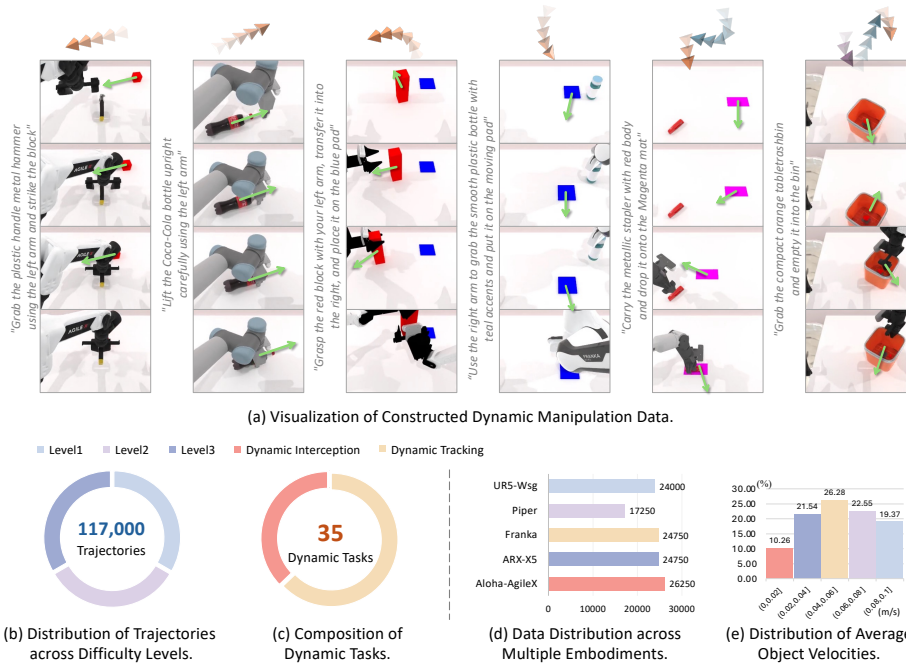


Fig. 2: Dataset Visualization. We present DOMINO dataset of 117,000 dynamic manipulation trajectories, covering 35 distinct tasks across five robot embodiments.

(e.g., RGB-D) and proprioception. The continuous action $\mathbf{a}_t \in \mathcal{A}$ specifies the dual-arm control commands. In dynamic environments, the transition dynamics $\mathcal{T}(s_{t+1}|s_t, \mathbf{a}_t)$ are inherently time-varying, governed by both the independent motion of the object and the interaction dynamics induced by robot contact.

Our objective is to learn a policy $\pi_\phi(\mathbf{a}_t|o_{t-h:t})$ that minimizes the expected finite-horizon cost:

$$J(\phi) = \mathbb{E} \left[\sum_{k=0}^{H-1} \gamma^k \ell(s_{t+k}, \mathbf{a}_{t+k}) \right], \quad (1)$$

where $\gamma \in [0, 1)$ is the discount factor, subject to safety constraints. The cost $\ell(\cdot)$ penalizes the spatial discrepancy between the end-effectors and the object, alongside the control effort. To achieve precise spatiotemporal interception, π_ϕ must implicitly anticipate future object states from historical observations.

2.2 Data Construction

To systematically evaluate generalizable dynamic manipulation, we introduce DOMINO. Unlike existing datasets focused on stationary tasks, DOMINO provides a scalable, low-cost pipeline for generating diverse dynamic data. As shown in Fig. 2, it comprises 35 dynamic tasks across five robot embodiments. To facilitate rigorous generalization assessments, we provide over 110K expert trajectories collected under both canonical and domain-randomized settings.

Constructing dynamic environments poses a significant challenge, primarily due to the strict spatiotemporal synchronization required between moving targets and robotic actions. Building upon the SAPIEN [55] physics engine and the RoboTwin 2.0 [10] framework, our data generation pipeline introduces a two-stage spatiotemporal synchronization method to reliably acquire expert demonstrations. First, in the temporal dry-run phase, we randomly sample the manipulation pose of the target object and execute the task in a static environment to record the exact execution time required by the robot arms. Next, in the kinematic back-calculation phase, we reverse-engineer the object’s initial spatial position based on the recorded execution time and specified motion trajectory. During the final dynamic execution, target objects are instantiated as kinematic bodies within SAPIEN. This ensures stable and predictable motion execution, immune to unintended physical disturbances. Furthermore, to guarantee expert data quality, we implement specialized adaptations for complex objects and enforce strict dynamic task-success criteria during automated generation.

2.3 Data Characteristics

DOMINO categorizes dynamic manipulation through a spatiotemporal task taxonomy, hierarchical motion complexities, and comprehensive evaluation metrics.

Spatiotemporal Task Taxonomy. To decouple the core challenges of dynamic manipulation from task-specific details, we divide the 35 benchmark tasks into two functional categories based on interaction requirements: dynamic interception and dynamic tracking. Dynamic interception focuses on instantaneous target acquisition, where the agent transitions from free space to establish contact with a moving target. This evaluates predictive kinematics and latency compensation. For example, catching a thrown object requires precise trajectory planning to reach an optimal interception point. Isolating this discrete action assesses the agent’s spatial precision under strict temporal constraints. In contrast, dynamic tracking involves continuous synchronization, requiring the agent to maintain a consistent spatial relationship with a moving target over a time window $\Delta\tau$. This evaluates real-time closed-loop control and velocity-matching capabilities, such as placing an object into a box on a conveyor belt. Consequently, this formulation assesses agent’s capacity for sustained error correction and trajectory adjustment during continuous interactions.

Hierarchical Dynamic Complexity. To evaluate agents across diverse dynamic complexities, ranging from predictable tracking to reactive adaptation, we categorize the motion dynamics \mathcal{F} into three levels, as illustrated in Fig. 1(a):

- Level 1 (Predictable Low-Order Dynamics): Objects move with a constant velocity $\mathbf{v} \sim \mathcal{U}(v_{\min}, v_{\max})$. This zero-curvature trajectory serves as a foundational test for instantaneous state estimation and linear extrapolation.
- Level 2 (Predictable High-Order Dynamics): Trajectories follow a polynomial curve $\mathbf{x}(t) = \sum_{k=0}^n \mathbf{b}_k (t/T_{traj})^k$ of degree $n \in [2, 5]$, fit to randomly sampled spatial control points. This introduces variable curvature and acceleration, requiring the agent to aggregate historical observations to implicitly model the physical dynamics.

- Level 3 (Stochastic and Abrupt Dynamics): Trajectories comprise $s \in [2, 3]$ independent segments of Level 1/2 dynamics, with segment durations drawn from a Dirichlet distribution. Velocity and acceleration are typically discontinuous at segment transitions. This unpredictability evaluates reactive robustness, compelling agent to rely on high-frequency closed-loop feedback.

Comprehensive Evaluation Metrics. To assess robustness across dynamic difficulties, we introduce the benchmark variant DOMINO@ α . This variant parameterizes the maximum target speed in meters per second using a scalar coefficient $\alpha \geq 0$. For instance, $\alpha = 0.1$ denotes a maximum speed of 0.1 m/s, and $\alpha = 0$ represents a static setting. Under this setting, we measure the Success Rate (SR), defined as the percentage of episodes that satisfy all task conditions within a time budget T_{\max} . As SR alone is insufficient for stochastic environments, we introduce the Manipulation Score (MS), a continuous metric designed to capture execution quality. The MS consists of a base Route Completion (RC) score adjusted by penalty factors. RC quantifies spatial convergence via a progress ratio $\rho = 1 - \|\mathbf{p}_{\text{ee}}^{(T_{\text{end}})} - \mathbf{p}_{\text{obj}}^{(T_{\text{end}})}\|_2 / \|\mathbf{p}_{\text{ee}}^{(0)} - \mathbf{p}_{\text{obj}}^{(0)}\|_2$, where \mathbf{p}_{ee} and \mathbf{p}_{obj} denote positions of the end-effector and target object at initial (0) and final (T_{end}) timesteps. For dual-arm setups, $RC \in [0, 100]$ reflects the maximum progress of either arm, computed as $100 \times \max(\rho_{\text{left}}, \rho_{\text{right}})$, with successful episodes assigned 100. Finally, to penalize unsafe behaviors, the overall MS is calculated by multiplying RC by 0.5 if the target exits the safe workspace or field of view, and by 0.8 upon collision with environmental clutter.

3 Dynamic-Aware VLA

To achieve generalizable dual-arm manipulation in dynamic environments, we propose the **Predictive Unified Manipulation Architecture (PUMA)** as shown in Fig. 3. Dynamic awareness requires capturing the historical context of objects and anticipating their future motion. Therefore, PUMA couples scene-centric history-aware perception with short-horizon object-centric prediction to satisfy spatiotemporal constraints induced by object dynamics \mathcal{F} within Qwen3-VL [1]. Given an observation history $o_{t-h:t}$ of length $h+1$ and a language instruction l , the model M_θ uses a shared backbone to jointly optimize action policy π_ϕ and an auxiliary future feature predictor ψ_ω . Specifically, it outputs an action chunk $\hat{\mathbf{a}}_{t:t+K-1}$ of length K in a single forward pass [63] alongside auxiliary features $\mathbf{z}_{t+1:t+N}$ of horizon N encoding future object motion. Crucially, the auxiliary future predictor is supervised only during training. This encourages shared representation to anticipate the dynamics \mathcal{F} and effectively regularizes policy without adding computational overhead during inference.

3.1 Scene-Centric Spatiotemporal Dynamics Encoding

To effectively operate in dynamic environments, our model requires a comprehensive understanding of both spatial context and temporal evolution. Therefore, the input space comprises three key components: a long-term language instruction, current multi-view observations, and a historical dynamic context.

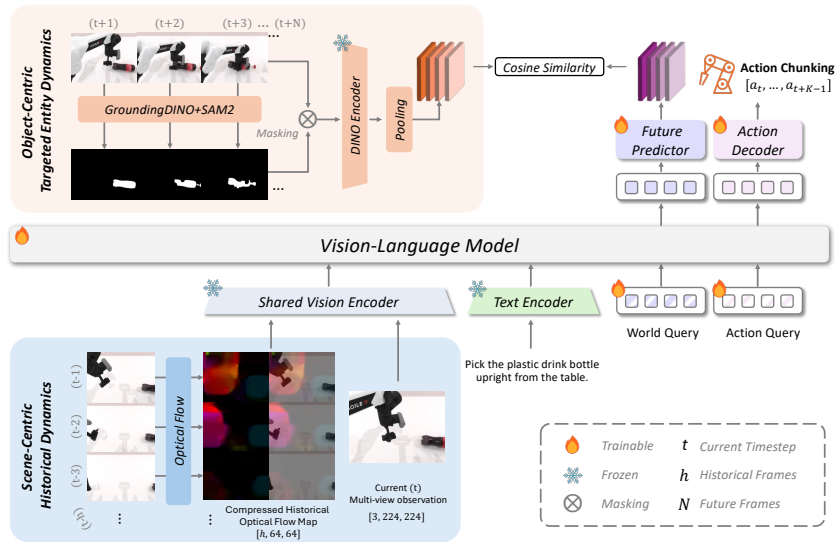


Fig. 3: PUMA processes historical motion flows, current observations, and instructions to encode scene-centric historical dynamics. It employs a dual-query mechanism where Action Queries decode continuous action chunks and World Queries aggregate dynamic representations. During training, world queries are supervised via a similarity loss against future features extracted by DINO to predict object-centric dynamics.

The language instruction l acts as the overarching task specification, guiding the manipulation policy. Concurrently, the current multi-view images serve as spatial visual prompts, providing dense observations of the immediate workspace. Capturing historical scene dynamics is crucial for reacting to moving objects.

To efficiently encode this dynamics, we introduce a compact dynamic context representation. We sample h historical third-person frames at a fixed stride and apply a spatial compression operator. Instead of directly stacking raw historical frames, which forces the network to implicitly deduce temporal changes, we compute optical flow maps across these compressed frames. Optical flow provides intuitive and explicit motion states, making it significantly easier for the policy to learn dynamic patterns. These flow maps are processed alongside the current multi-view visual input through Qwen3-VL visual encoder, forming the observation history $o_{t-h:t}$ that supplies the model with explicit dense motion cues. This design supplies the model with explicit dense motion cues, enabling the policy to accurately estimate object motion trends.

3.2 Object-Centric Dynamic Representation

To effectively interact within dynamic environments, the policy must explicitly anticipate the future motion of target objects. While existing vision-language-action frameworks [61] attempt to forecast comprehensive scene-level dynamic regions, we posit that generalizable dynamic manipulation necessitates an object-centric focus, isolating the target’s trajectory from irrelevant scene dynamics. To construct an accurate supervision signal for this predictive capability, we

sample N future frames $I_{t+1:t+N}$ at a fixed interval during training and isolate the target object’s state using a frozen grounding module [46]. Specifically, the manipulated object parsed from the language instruction serves as a text prompt p for GroundingDINO [31], which generates a target bounding box. This box is then processed by SAM2 [44] to yield a precise segmentation mask. Let $\mathcal{B}(I, p)$ denote resulting binary mask, $\mathcal{E}(I)$ denote frozen DINO patch-token encoder, and $\mathcal{P}(\cdot, \cdot)$ denote masked average pooling. The object-centric future feature \mathbf{f}_{t+i} is computed as:

$$\mathbf{f}_{t+i} = \mathcal{P}(\mathcal{E}(I_{t+i}), \mathcal{B}(I_{t+i}, p)), \quad i = 1, \dots, N. \quad (2)$$

To model these future states, we introduce N learnable world queries that aggregate the spatiotemporal context to predict the target’s future representations within the latent space. We then optimize these predictions by enforcing a similarity loss against the extracted ground-truth DINO features. This explicit supervision forces the latent world representation to capture and anticipate the underlying object dynamics. This supervision is applied only during training, requiring no future frames at inference.

3.3 Training Strategy

We train the unified model M_θ end-to-end using supervised behavioral cloning combined with an auxiliary future-feature prediction objective. Each training tuple comprises $\{o_{t-h:t}, l, \mathbf{f}_{t+1:t+N}, \mathbf{a}_{t:t+K-1}^*\}$. The action policy is supervised via an ℓ_1 regression loss over the predicted action chunk:

$$\mathcal{L}_{action} = \frac{1}{K} \sum_{i=0}^{K-1} \|\hat{\mathbf{a}}_{t+i} - \mathbf{a}_{t+i}^*\|_1. \quad (3)$$

Simultaneously, the auxiliary future predictor is optimized by minimizing the cosine distance between the predicted representations \mathbf{z}_{t+i} and the ground-truth object-centric features \mathbf{f}_{t+i} :

$$\mathcal{L}_{world} = \frac{1}{N} \sum_{i=1}^N \left(1 - \frac{\mathbf{z}_{t+i}^\top \mathbf{f}_{t+i}}{\|\mathbf{z}_{t+i}\|_2 \|\mathbf{f}_{t+i}\|_2} \right). \quad (4)$$

Overall training objective is formulated as a weighted sum of two components:

$$\mathcal{L}_{total} = \mathcal{L}_{action} + \lambda \mathcal{L}_{world}, \quad (5)$$

where λ is a balancing hyperparameter controlling influence of dynamics task.

4 Experiment

All VLA models are trained on NVIDIA A100 GPUs, while data generation and evaluation are performed on NVIDIA RTX GPUs. Appendix provides additional implementation details and hyperparameters. To balance broad experimental coverage with limited compute, unless otherwise stated, all experiments are conducted in clean setting with the Aloha-AgileX robot, using a training mixture of 35 dynamic tasks under Level 1 dynamics with dynamic coefficient $\alpha = 0.1$.

4.1 Experimental Setup

Benchmarks. We primarily evaluate on our proposed DOMINO@0.1 benchmark, reporting the Success Rate (SR) and Manipulation Score (MS). Additionally, we provide selected results in static environments using RoboTwin 2.0 [10].

Baselines. We evaluate PUMA against the standard policy learning framework ACT [63] and several state-of-the-art VLA models, including OpenVLA [25], OpenVLA-OFT [24], RDT [32], π_0 [5], $\pi_{0.5}$ [4], π_0 -FAST [40], VLA-Adapter [52], InternVLA-M1 [12], and Qwen3-VL-based VLAs [11]. For a fair comparison, all baselines are fine-tuned on proposed DOMINO dataset. Note that while the VLA models are fine-tuned across all tasks, ACT is fine-tuned on a per-task basis.

4.2 Challenges of the Proposed DOMINO Dataset

Table 1: Quantitative evaluation of VLA models in static and our proposed DOMINO. $X \rightarrow Y$ denotes training in environment X and testing in Y (S: static, D: dynamic), with ZS representing zero-shot evaluation and FT indicating fine-tuning. Subscripts denote performance Δ (ZS vs. Static; FT vs. ZS).

Simulation Task	ACT [63]			OpenVLA-OFT [24]			$\pi_{0.5}$ [4]		
	Static S→S	ZS S→D	FT D→D	Static S→S	ZS S→D	FT D→D	Static S→S	ZS S→D	FT D→D
<i>Adjust Bottle</i>	97%	37%	65%	47%	16%	58%	92%	12%	52%
<i>Click Alarmclock</i>	29%	3%	8%	57%	9%	6%	48%	8%	14%
<i>Grab Roller</i>	95%	24%	23%	47%	24%	28%	98%	6%	10%
<i>Handover Block</i>	43%	0%	11%	3%	3%	9%	2%	0%	1%
<i>Handover Mic</i>	82%	13%	23%	93%	8%	25%	63%	7%	5%
<i>Move Can Pot</i>	23%	0%	26%	34%	29%	29%	14%	5%	7%
<i>Move Pillbottle Pad</i>	1%	0%	1%	1%	0%	1%	20%	5%	6%
<i>Place Bread Skillet</i>	9%	5%	12%	4%	1%	1%	39%	5%	9%
<i>Place Fan</i>	0%	0%	1%	3%	0%	1%	30%	1%	2%
<i>Place Object Basket</i>	18%	19%	21%	19%	16%	18%	57%	6%	11%
.....(35 tasks)									
<i>Press Stapler</i>	31%	2%	4%	35%	2%	5%	35%	1%	6%
<i>Rotate QRcode</i>	3%	0%	0%	10%	8%	11%	54%	2%	4%
<i>Scan Object</i>	1%	2%	2%	0%	0%	4%	7%	0%	1%
<i>Shake Bottle</i>	74%	18%	14%	63%	12%	17%	95%	19%	33%
<i>Shake Bottle Horiz.</i>	63%	23%	18%	57%	19%	31%	97%	24%	42%
Average (%)	27.7	6.5 _{-21.2}	9.4 _{+2.9}	17.5	6.7 _{-10.8}	9.1 _{+2.4}	44.8	7.5 _{-37.3}	9.6 _{+2.1}

To investigate the challenges of dynamic environments, we evaluate representative VLA architectures in both static and dynamic settings. As shown in Tab. 1, these models exhibit satisfactory performance in static scenarios (S→S), but their performance degrades significantly in dynamic environments (S→D). Under identical task settings with moving targets, the average success rate drops drastically. For instance, the performance of $\pi_{0.5}$ [4] falls from 44.8% to 7.5%.

Furthermore, we explore whether fine-tuning these baselines with dynamic data

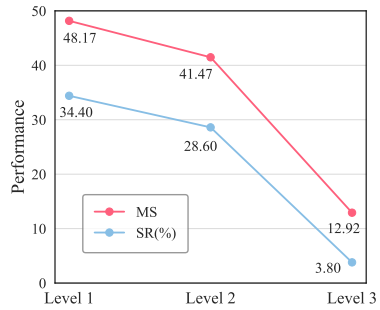


Fig. 4: Performance degradation of the ACT model across three dynamic complexity.

Table 2: Results of explicitly modeling future trajectories.

Method	Settings	w/ GT Traj.	SR (%)↑	MS↑
OpenVLA-OFT [24]	Static	×	17.51	17.51
	Dynamic	×	9.06	24.06
	Dynamic	✓	10.33	32.00

(D→D) can bridge this gap. We observe only marginal improvements, with average success rates increasing by less than 3%. We attribute this bottleneck to fundamental architectural limitations rather than mere data distribution shifts. Standard VLA architectures rely on single-frame observations, inherently limiting their dynamic awareness. We argue that effective dynamic manipulation requires *capturing historical object context and anticipating future motion*. The current VLA paradigm lacks these essential dynamic modeling capabilities, resulting in sub-optimal dynamic manipulation performance.

While our primary experiments focus on Level 1 dynamics, we also investigate the impact of higher dynamic complexities. We train ACT models per-task on five tasks and evaluate them across all three dynamic levels. As illustrated in Fig. 4, performance deteriorates rapidly as complexity increases. Level 2 and Level 3 environments are significantly more challenging than Level 1, highlighting the need for stronger dynamic modeling architectures in future research.

Finding 1: *Dynamic manipulation presents a challenging new frontier.* The transition from static to dynamic environments introduces complex spatiotemporal challenges that fundamentally degrade the reliability of existing paradigms. It represents a distinct and demanding domain that cannot be solved by merely scaling static manipulation approaches.

To validate this hypothesis and isolate the performance bottleneck of current VLAs, we conduct an oracle experiment, as detailed in Tab. 2. We introduce an auxiliary dynamic ground-truth encoder, implemented as an MLP. This encoder takes the target object’s future pose window combined with a continuous trajectory parameter vector as input to generate a dynamic conditional representation. During the forward pass, this conditional vector is concatenated with the action queries and passed through a subsequent MLP layer. Experimental results reveal a nuanced behavior: while the explicit introduction of future trajectories yields only a marginal improvement in overall SR, it significantly boosts MS. Qualitative analysis of the evaluation rollouts indicates that the policy successfully acquires and tracks the correct trajectory but exhibits control jitter and temporal inconsistency during the actual manipulation phase. We attribute this to the lack of historical frame observations; without historical context, the model fails to comprehend the target’s underlying physical dynamics. Instead, the policy overfits to naive trajectory following, which inadvertently interferes with closed-loop manipulation learning. However, in successful episodes, the introduction of ground-truth trajectories yields exceptionally high manipulation quality that approaches expert demonstrations, confirming the potential of future spatial cues if appropriately grounded in physical context.

Table 3: Comparison with SOTA methods on DOMINO.

Method	Venue	LLM	SR (%) \uparrow	MS \uparrow
OpenVLA [25]	CoRL 24	Llama-2	1.54	6.10
RDT-1B [32]	ICLR 25	DiT-1B	5.34	17.71
π_0 [5]	RSS 25	PaliGemma	8.17	23.96
$\pi_{0.5}$ [4]	CoRL 25	PaliGemma	9.63	26.17
InternVLA-M1 [12]	arXiv 25	InternVL	5.40	27.57
Isaac-GR00T [3]	arXiv 25	Qwen3-VL*	6.10	28.60
VLA-Adapter [52]	AAAI 26	Qwen3-VL	4.40	24.31
π_0 -FAST [40]	RSS 25	PaliGemma	3.54	20.87
		Qwen3-VL*	5.74	20.66
OpenVLA-OFT [24]	RSS 25	Llama-2	9.06	24.06
		Qwen3-VL*	10.86	30.49
PUMA (OURS)	-	Qwen3-VL	17.20	34.97

* Methods with Qwen3-VL backbones are our re-implementations for fair comparison.

Finding 2: Naive future trajectory injection is insufficient for dynamic manipulation. While providing future spatial cues improves motion tracking, the absence of historical observations prevents the model from understanding physical dynamics, leading to control instability during manipulation. Effective dynamic manipulation requires a holistic integration of both historical context and future anticipation.

4.3 Effectiveness of Dynamic-Aware VLA

Building upon the insight that effective dynamic manipulation requires both historical context and future anticipation, we evaluate PUMA as a solution to these spatiotemporal challenges. As shown in Tab. 3, PUMA demonstrates a performance advantage over SOTA VLA models on dynamic manipulation tasks.

Specifically, PUMA achieves the highest average success rate of 17.20%, substantially outperforming recent strong baselines such as OpenVLA-OFT (Qwen3-VL-based) [11] (10.90%) and $\pi_{0.5}$ [4] (9.63%). Furthermore, our method attains a peak Manipulation Score of 34.97, indicating a higher quality of interaction with moving targets. We attribute this performance leap to the explicit integration of historical observation frames and the introduction of the auxiliary future feature predictor ψ_ω . By forcing shared representation to anticipate object dynamics during training, model learns to infer future states of moving objects during inference. This design effectively mitigates the dynamic awareness bottleneck identified in previous section.

To provide a detailed task-level comparison, we visualize the performance breakdown across individual manipulation tasks in Fig. 5. Notably, PUMA yields

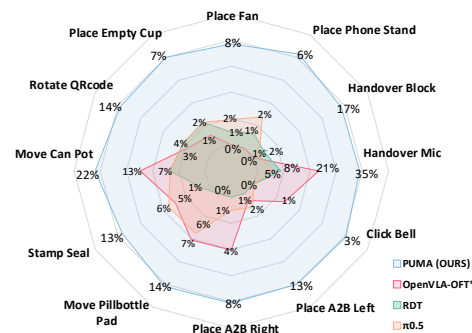
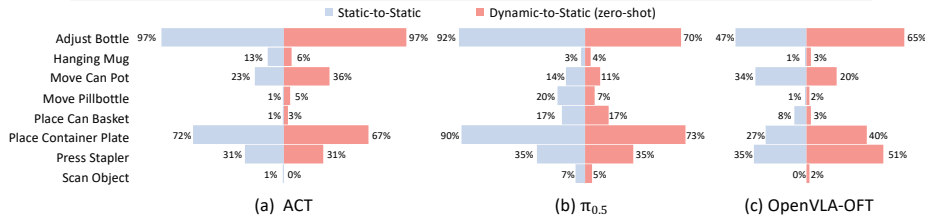


Fig. 5: PUMA performs significantly better than other baselines on difficult tasks.

Notably, PUMA yields

Table 4: Comparison between co-training and dynamic data training. * indicates our reproduction of OpenVLA-OFT [11] utilizing the same Qwen3-VL backbone to ensure fairness. To strictly isolate the performance gains yielded by data mixing, PUMA is evaluated under a controlled configuration (prediction horizon $N = 2$).

Method	Static	Dynamic	SR (%) \uparrow	MS \uparrow
OpenVLA-OFT* [11]	×	✓	10.86	30.49
	✓	✓	12.89 $_{+2.03}$	30.80 $_{+0.31}$
PUMA	×	✓	14.80	32.74
	✓	✓	19.71 $_{+4.91}$	37.76 $_{+5.02}$



The model trained on DOMINO (coral) demonstrates generalization ability when tested in zero-shot scenarios to static scenes, and achieves comparable results to static data (blue) in some tasks.

substantial improvements on highly challenging dynamic tasks where baseline methods struggle and achieve only marginal success rates. These pronounced performance gains underscore robustness of our approach in handling complex object dynamics. Overall, the quantitative results validate that our unified, dynamics-aware design represents an effective step toward generalizable manipulation in dynamic environments.

4.4 The Role of Dynamic Data in Generalization

To investigate the generalization capability of dynamic data, we evaluate the zero-shot performance of policies trained exclusively on dynamic datasets when deployed in static environments. As shown in the bar charts of Tab. 4, dynamic-trained models achieve comparable performance to their static-trained counterparts on certain tasks. For instance, using the OpenVLA-OFT baseline, the dynamic-trained policy outperforms the static-trained policy on Adjust Bottle (65% vs. 47%) and Place Container Plate (40% vs. 27%) tasks, while maintaining parity on Adjust Bottle task (97%) under ACT baseline. This indicates that tracking and interacting with moving targets subsumes skills required for static manipulation, effectively mitigating overfitting to stationary configurations.

Furthermore, we evaluate co-training policies on mixed static and dynamic datasets. As detailed in Tab. 4, this hybrid training strategy yields significant performance improvements in dynamic environments. Specifically, for PUMA, incorporating static data increases the overall SR by 4.91% (from 14.80% to 19.71%) and the MS by 5.02 compared to training on dynamic data alone. We hypothesize that this synergy arises because static data provides stable structural priors for foundational manipulation, while dynamic data introduces the spatiotemporal variations necessary for reactive dexterity.

Finding 3: *Dynamic data fosters generalizable representations.* Exposure to dynamic interactions mitigates overfitting to static positional biases, encouraging the policy to learn robust spatiotemporal representations. This facilitates effective zero-shot transfer to static environments and, when co-trained with static data, maximizes dynamic manipulation performance by combining stable foundational priors with reactive dexterity.

Table 5: Ablation of core components and future prediction steps (N). We evaluate the impact of historical representations (Hist. Rep.), auxiliary future prediction (Aux. Pred.), and the horizon of prediction in dynamic environments.

Method	Components			SR (%) \uparrow	MS \uparrow
	Hist. Rep.	Aux. Pred.	Steps (N)		
Baseline	×	×	-	10.86	30.49
+ Hist. Flow	✓	×	-	11.71	31.02
+ Hist. Flow	✓	✓	2	14.80	32.74
+ Hist. Frames	✓	✓	2	8.15	28.62
+ Hist. Flow	✓	✓	4	17.20	34.97

4.5 Ablation Study

We conduct an ablation study to evaluate our proposed modules, as detailed in Tab. 5. First, providing explicit motion cues via optical flow (+ Hist. Flow) improves the baseline SR from 10.86% to 11.71%. Adding the auxiliary future prediction task at $N = 2$ (+ Hist. Flow with Aux. Pred.) further boosts the SR to 14.80%, confirming that anticipating future states effectively regularizes the action policy. Crucially, replacing optical flow with raw historical frames (+ Hist. Frames) degrades the SR to 8.10%, demonstrating that implicitly deducing temporal dynamics from raw frames is suboptimal compared to utilizing explicit flow representations. Finally, extending the prediction horizon to $N = 4$ achieves the best performance (17.20% SR, 34.97 MS), suggesting that a longer anticipation horizon enables a more robust understanding of future trajectories.

5 Related Work

5.1 Vision-Language-Action Model

Vision-Language-Action models [2, 6, 45, 48, 59, 66] have transformed robotic manipulation by directly mapping multimodal inputs and instructions into control commands. Recent architectures [3–5, 12, 24, 25, 32] leverage mechanisms like diffusion policies to achieve robust zero-shot adaptability. However, their application in dynamic real-world environments is bottlenecked by inadequate spatiotemporal modeling. Regarding temporal modeling, the high computational cost of processing multi-frame observations forces most VLAs to operate as memoryless single-frame policies. This precludes the extraction of continuous dynamics. While recent efforts incorporate temporal contexts [8, 14, 16, 20, 39, 50] or memory mechanisms for long-horizon tasks [19, 26, 28, 30, 47, 64], they primarily

track task progression. They fail to perform high-frequency motion estimation required for dynamic manipulation. In terms of spatial representation, standard VLAs assume static environments and neglect the continuous motion of manipulated objects [43]. Approaches like ReconVLA [49] allocate visual attention to target objects. DreamVLA [61] integrated dream query to predict global scene transitions. However, these methods lack the fine-grained object-centric dynamic modeling essential for reactive planning. Furthermore, existing dynamic manipulation methods [53, 62] are typically restricted to simplified motion tasks and fail to capture real-world dynamic complexity. To bridge these gaps, we introduces spatiotemporal designs to effectively tackle dynamic manipulation tasks.

5.2 Datasets and Benchmarks for Robotic Manipulation

Robot learning benchmarks primarily encompass real-world and simulation environments. While real-world platforms [7, 23, 38, 51, 54, 56] enable standardized training and evaluation on physical robots, they are often hindered by limited reproducibility, hardware variations, and safety constraints. Consequently, simulated closed-loop environments remain indispensable for scalable and reliable policy evaluation [15, 21, 34, 36, 41, 58, 65]. In simulation, foundational benchmarks like RL Bench [18] and CALVIN [35] established multi-task, long-horizon evaluation. Subsequent platforms address diverse challenges: LIBERO [29] for lifelong knowledge transfer, and RoboCasa [37] for generative task scaling. Furthermore, The Colosseum [42] and SIMPLER [27] evaluate out-of-distribution robustness, while RoboTwin2.0 [10] and VLABench [60] explore bimanual coordination and cognitive reasoning. However, existing simulation benchmarks fundamentally rely on a static world assumption where state transitions are strictly robot-driven, failing to assess the manipulation of independently moving targets. To address this, we introduces a comprehensive benchmark designed to evaluate generalizable dual-arm manipulation capabilities in dynamic environments.

6 Conclusion

In this work, we identify and address a critical gap in embodied AI: generalizable robotic manipulation in dynamic environments. To systematically investigate this underexplored frontier, we introduce DOMINO, a scalable benchmark featuring diverse dual-arm tasks, hierarchical motion complexities, and a comprehensive multidimensional evaluation framework. Our empirical analysis reveals that current VLA paradigms inherently lack dynamic awareness, failing to integrate historical physical context with future motion anticipation. To overcome these spatiotemporal limitations, we propose PUMA. By incorporating scene-centric historical optical flow and an auxiliary object-centric future prediction objective, PUMA effectively anticipates target trajectories and significantly outperforms state-of-the-art baselines in complex dynamic scenarios. Furthermore, our findings demonstrate that training with dynamic data not only enhances reactive dexterity but also fosters robust spatiotemporal representations that generalize seamlessly to static tasks. We hope DOMINO and PUMA serve as foundational stepping stones toward highly reactive and robust embodied intelligence in complex, real-world dynamic environments.

References

1. Bai, S., Cai, Y., Chen, R., Chen, K., Chen, X., Cheng, Z., Deng, L., Ding, W., Gao, C., Ge, C., Ge, W., Guo, Z., Huang, Q., Huang, J., Huang, F., Hui, B., Jiang, S., Li, Z., Li, M., Li, M., Li, K., Lin, Z., Lin, J., Liu, X., Liu, J., Liu, C., Liu, Y., Liu, D., Liu, S., Lu, D., Luo, R., Lv, C., Men, R., Meng, L., Ren, X., Ren, X., Song, S., Sun, Y., Tang, J., Tu, J., Wan, J., Wang, P., Wang, P., Wang, Q., Wang, Y., Xie, T., Xu, Y., Xu, H., Xu, J., Yang, Z., Yang, M., Yang, J., Yang, A., Yu, B., Zhang, F., Zhang, H., Zhang, X., Zheng, B., Zhong, H., Zhou, J., Zhou, F., Zhou, J., Zhu, Y., Zhu, K.: Qwen3-vl technical report. arXiv preprint arXiv:2511.21631 (2025) [6](#), [21](#)
2. Belkhal, S., Ding, T., Xiao, T., Sermanet, P., Vuong, Q., Tompson, J., Chebotar, Y., Dwibedi, D., Sadigh, D.: Rt-h: Action hierarchies using language. arXiv preprint arXiv:2403.01823 (2024) [13](#)
3. Bjorck, J., Castañeda, F., Cherniadev, N., Da, X., Ding, R., Fan, L., Fang, Y., Fox, D., Hu, F., Huang, S., et al.: Gr00t n1: An open foundation model for generalist humanoid robots. arXiv preprint arXiv:2503.14734 (2025) [1](#), [11](#), [13](#)
4. Black, K., Brown, N., Darpinian, J., Dhabalia, K., Driess, D., Esmail, A., Equi, M.R., Finn, C., Fusai, N., Galliker, M.Y., et al.: $\pi_{0.5}$: a vision-language-action model with open-world generalization. In: 9th Annual Conference on Robot Learning (2025) [1](#), [9](#), [11](#), [13](#), [26](#), [28](#), [29](#), [30](#), [31](#)
5. Black, K., Brown, N., Driess, D., Esmail, A., Equi, M., Finn, C., Fusai, N., Groom, L., Hausman, K., Ichter, B., et al.: π_0 : A vision-language-action flow model for general robot control. arXiv preprint arXiv:2410.24164 (2024) [1](#), [3](#), [9](#), [11](#), [13](#), [26](#)
6. Brohan, A., Brown, N., Carbajal, J., Chebotar, Y., Dabis, J., Finn, C., Gopalakrishnan, K., Hausman, K., Herzog, A., Hsu, J., et al.: Rt-1: Robotics transformer for real-world control at scale. Robotics: Science and Systems XIX (2023) [2](#), [13](#)
7. Bu, Q., Cai, J., Chen, L., Cui, X., Ding, Y., Feng, S., Gao, S., He, X., Hu, X., Huang, X., et al.: Agibot world colosseo: A large-scale manipulation platform for scalable and intelligent embodied systems. arXiv preprint arXiv:2503.06669 (2025) [14](#)
8. Bu, Q., Yang, Y., Cai, J., Gao, S., Ren, G., Yao, M., Luo, P., Li, H.: Uni-vla: Learning to act anywhere with task-centric latent actions. arXiv preprint arXiv:2505.06111 (2025) [13](#)
9. Cen, J., Yu, C., Yuan, H., Jiang, Y., Huang, S., Guo, J., Li, X., Song, Y., Luo, H., Wang, F., et al.: Worldvla: Towards autoregressive action world model. arXiv preprint arXiv:2506.21539 (2025) [3](#)
10. Chen, T., Chen, Z., Chen, B., Cai, Z., Liu, Y., Li, Z., Liang, Q., Lin, X., Ge, Y., Gu, Z., et al.: Robotwin 2.0: A scalable data generator and benchmark with strong domain randomization for robust bimanual robotic manipulation. arXiv preprint arXiv:2506.18088 (2025) [2](#), [5](#), [9](#), [14](#), [21](#)
11. starVLA Contributors: Starvla: A lego-like codebase for vision-language-action model developing. GitHub repository (1 2025). <https://doi.org/10.5281/zenodo.18264214>, <https://github.com/starVLA/starVLA> [9](#), [11](#), [12](#), [27](#)
12. Contributors, I.M.: Internvla-m1: A spatially guided vision-language-action framework for generalist robot policy. arXiv preprint arXiv:2510.13778 (2025) [9](#), [11](#), [13](#), [25](#), [26](#)
13. Cui, C., Ding, P., Song, W., Bai, S., Tong, X., Ge, Z., Suo, R., Zhou, W., Liu, Y., Jia, B., Zhao, H., Huang, S., Wang, D.: Openhelix: A short survey, empirical analysis, and open-source dual-system vla model for robotic manipulation. arXiv preprint arXiv:2505.03912 (2025) [1](#)

14. Driess, D., Xia, F., Sajjadi, M.S., Lynch, C., Chowdhery, A., Ichter, B., Wahid, A., Tompson, J., Vuong, Q., Yu, T., et al.: Palm-e: An embodied multimodal language model. In: International Conference on Machine Learning. pp. 8469–8488. PMLR (2023) [13](#)
15. Ehsani, K., Han, W., Herrasti, A., VanderBilt, E., Weihs, L., Kolve, E., Kembhavi, A., Mottaghi, R.: Manipulathor: A framework for visual object manipulation. In: Proceedings of the IEEE/CVF conference on computer vision and pattern recognition. pp. 4497–4506 (2021) [14](#)
16. Fan, C., Jia, X., Sun, Y., Wang, Y., Wei, J., Gong, Z., Zhao, X., Tomizuka, M., Yang, X., Yan, J., et al.: Interleave-vla: Enhancing robot manipulation with interleaved image-text instructions. arXiv preprint arXiv:2505.02152 (2025) [13](#)
17. Farnebäck, G.: Two-frame motion estimation based on polynomial expansion. In: Scandinavian conference on Image analysis. pp. 363–370. Springer (2003) [23](#)
18. James, S., Ma, Z., Rovick Arrojo, D., Davison, A.J.: Rlbench: The robot learning benchmark & learning environment. IEEE Robotics and Automation Letters (2020) [14](#)
19. Jang, H., Yu, S., Kwon, H., Jeon, H., Seo, Y., Shin, J.: Contextvla: Vision-language-action model with amortized multi-frame context. arXiv preprint arXiv:2510.04246 (2025) [13](#)
20. Jiang, Y., Gupta, A., Zhang, Z., Wang, G., Dou, Y., Chen, Y., Fei-Fei, L., Anandkumar, A., Zhu, Y., Fan, L.: Vima: Robot manipulation with multimodal prompts. In: International Conference on Machine Learning. pp. 14975–15022. PMLR (2023) [13](#)
21. Jiang, Z., Xie, Y., Lin, K., Xu, Z., Wan, W., Mandlekar, A., Fan, L.J., Zhu, Y.: Dexmimicgen: Automated data generation for bimanual dexterous manipulation via imitation learning. In: 2025 IEEE International Conference on Robotics and Automation (ICRA). pp. 16923–16930. IEEE (2025) [14](#)
22. Kaelbling, L.P., Littman, M.L., Cassandra, A.R.: Planning and acting in partially observable stochastic domains. Artificial intelligence **101**(1-2), 99–134 (1998) [3](#)
23. Khazatsky, A., Pertsch, K., Nair, S., Balakrishna, A., Dasari, S., Karamcheti, S., Nasiriany, S., Srirama, M.K., Chen, L.Y., Ellis, K., et al.: Droid: A large-scale in-the-wild robot manipulation dataset. In: Robotics: Science and Systems (2024) [14](#)
24. Kim, M.J., Finn, C., Liang, P.: Fine-tuning vision-language-action models: Optimizing speed and success. arXiv preprint arXiv:2502.19645 (2025) [1](#), [9](#), [10](#), [11](#), [13](#), [24](#), [25](#), [28](#), [29](#), [30](#), [31](#)
25. Kim, M.J., Pertsch, K., Karamcheti, S., Xiao, T., Balakrishna, A., Nair, S., Rafailov, R., Foster, E.P., Sanketi, P.R., Vuong, Q., et al.: Openvla: An open-source vision-language-action model. In: 8th Annual Conference on Robot Learning [1](#), [3](#), [9](#), [11](#), [13](#), [24](#), [25](#)
26. Koo, M., Choi, D., Kim, T., Lee, K., Kim, C., Seo, Y., Shin, J.: Hamlet: Switch your vision-language-action model into a history-aware policy. arXiv preprint arXiv:2510.00695 (2025) [13](#)
27. Li, X., Hsu, K., Gu, J., Pertsch, K., Mees, O., Walke, H.R., Fu, C., Lunawat, I., Sieh, I., Kirmani, S., Levine, S., Wu, J., Finn, C., Su, H., Vuong, Q., Xiao, T.: Evaluating real-world robot manipulation policies in simulation. arXiv preprint arXiv:2405.05941 (2024) [14](#)
28. Lin, M., Ding, P., Wang, S., Zhuang, Z., Liu, Y., Tong, X., Song, W., Lyu, S., Huang, S., Wang, D.: Hif-vla: Hindsight, insight and foresight through motion representation for vision-language-action models. arXiv preprint arXiv:2512.09928 (2025) [13](#)

29. Liu, B., Zhu, Y., Gao, C., Feng, Y., Liu, Q., Zhu, Y., Stone, P.: Libero: Benchmarking knowledge transfer for lifelong robot learning. *Advances in Neural Information Processing Systems* **36**, 44776–44791 (2023) [14](#)
30. Liu, C., Zhang, J., Li, C., Zhou, Z., Wu, S., Huang, S., Duan, H.: Ttf-vla: Temporal token fusion via pixel-attention integration for vision-language-action models. *arXiv preprint arXiv:2508.19257* (2025) [13](#)
31. Liu, S., Zeng, Z., Ren, T., Li, F., Zhang, H., Yang, J., Li, C., Yang, J., Su, H., Zhu, J., et al.: Grounding dino: Marrying dino with grounded pre-training for open-set object detection. *arXiv preprint arXiv:2303.05499* (2023) [8](#), [23](#)
32. Liu, S., Wu, L., Li, B., Tan, H., Chen, H., Wang, Z., Xu, K., Su, H., Zhu, J.: Rdt-1b: a diffusion foundation model for bimanual manipulation. *arXiv preprint arXiv:2410.07864* (2024) [3](#), [9](#), [11](#), [13](#), [24](#), [25](#)
33. Loshchilov, I., Hutter, F.: Decoupled weight decay regularization. *International Conference on Learning Representations* (2019) [22](#)
34. Makoviychuk, V., Wawrzyniak, L., Guo, Y., Lu, M., Storey, K., Macklin, M., Hoeller, D., Rudin, N., Allshire, A., Handa, A., et al.: Isaac gym: High performance gpu based physics simulation for robot learning. In: *Thirty-fifth Conference on Neural Information Processing Systems Datasets and Benchmarks Track (Round 2)* [14](#)
35. Mees, O., Hermann, L., Rosete-Beas, E., Burgard, W.: Calvin: A benchmark for language-conditioned policy learning for long-horizon robot manipulation tasks. *IEEE Robotics and Automation Letters* **7**(3), 7327–7334 (2022) [14](#)
36. Mu, T., Ling, Z., Xiang, F., Yang, D.C., Li, X., Tao, S., Huang, Z., Jia, Z., Su, H.: Maniskill: Generalizable manipulation skill benchmark with large-scale demonstrations. In: *Thirty-fifth Conference on Neural Information Processing Systems Datasets and Benchmarks Track (Round 2)* [14](#)
37. Nasiriany, S., Maddukuri, A., Zhang, L., Parikh, A., Lo, A., Joshi, A., Mandlekar, A., Zhu, Y.: Robocasa: Large-scale simulation of everyday tasks for generalist robots. In: *Robotics: Science and Systems* (2024) [14](#)
38. O’Neill, A., Rehman, A., Maddukuri, A., Gupta, A., Padalkar, A., Lee, A., Pooley, A., Gupta, A., Mandlekar, A., Jain, A., et al.: Open x-embodiment: Robotic learning datasets and rt-x models: Open x-embodiment collaboration 0. pp. 6892–6903. *IEEE* (2024) [2](#), [14](#)
39. Patratskiy, M.A., Kovalev, A.K., Panov, A.I.: Spatial traces: Enhancing vla models with spatial-temporal understanding. *Optical Memory and Neural Networks* **34**(Suppl 1), S72–S82 (2025) [13](#)
40. Pertsch, K., Stachowicz, K., Ichter, B., Driess, D., Nair, S., Vuong, Q., Mees, O., Finn, C., Levine, S.: Fast: Efficient action tokenization for vision-language-action models. *arXiv preprint arXiv:2501.09747* (2025) [9](#), [11](#), [25](#), [26](#)
41. Puig, X., Undersander, E., Szot, A., Cote, M.D., Yang, T.Y., Partsey, R., Desai, R., Clegg, A.W., Hlavac, M., Min, S.Y., et al.: Habitat 3.0: A co-habitat for humans, avatars and robots. *arXiv preprint arXiv:2310.13724* (2023) [14](#)
42. Pumacay, W., Singh, I., Duan, J., Krishna, R., Thomason, J., Fox, D.: The colosseum: A benchmark for evaluating generalization for robotic manipulation. *arXiv preprint arXiv:2402.08191* (2024) [14](#)
43. Qiu, W., Huang, T., Feng, A., Ying, R.: Efficient long-horizon vision-language-action models via static-dynamic disentanglement. *arXiv preprint arXiv:2602.03983* (2026) [14](#)
44. Ravi, N., Gabeur, V., Hu, Y.T., Hu, R., Ryali, C., Ma, T., Khedr, H., Rädle, R., Rolland, C., Gustafson, L., Mintun, E., Pan, J., Alwala, K.V., Carion, N.,

- Wu, C.Y., Girshick, R., Dollár, P., Feichtenhofer, C.: Sam 2: Segment anything in images and videos (2024), <https://arxiv.org/abs/2408.00714> **8**, **23**
45. Reed, S., Zolna, K., Parisotto, E., Colmenarejo, S.G., Novikov, A., Barth-marion, G., Giménez, M., Sulsky, Y., Kay, J., Springenberg, J.T., et al.: A generalist agent. *Transactions on Machine Learning Research* **13**
 46. Ren, T., Liu, S., Zeng, A., Lin, J., Li, K., Cao, H., Chen, J., Huang, X., Chen, Y., Yan, F., Zeng, Z., Zhang, H., Li, F., Yang, J., Li, H., Jiang, Q., Zhang, L.: Grounded sam: Assembling open-world models for diverse visual tasks (2024) **8**, **23**
 47. Shi, H., Xie, B., Liu, Y., Sun, L., Liu, F., Wang, T., Zhou, E., Fan, H., Zhang, X., Huang, G.: Memoryvla: Perceptual-cognitive memory in vision-language-action models for robotic manipulation. *arXiv preprint arXiv:2508.19236* (2025) **1**, **13**
 48. Shridhar, M., Manuelli, L., Fox, D.: Cliport: What and where pathways for robotic manipulation. In: *Conference on robot learning*. pp. 894–906. PMLR (2022) **13**
 49. Song, W., Zhou, Z., Zhao, H., Chen, J., Ding, P., Yan, H., Huang, Y., Tang, F., Wang, D., Li, H.: Reconvla: Reconstructive vision-language-action model as effective robot perceiver. *arXiv preprint arXiv:2508.10333* (2025) **14**
 50. Team, O.M., Ghosh, D., Walke, H., Pertsch, K., Black, K., Mees, O., Dasari, S., Hejna, J., Kreiman, T., Xu, C., et al.: Octo: An open-source generalist robot policy. *arXiv preprint arXiv:2405.12213* (2024) **13**
 51. Walke, H.R., Black, K., Zhao, T.Z., Vuong, Q., Zheng, C., Hansen-Estruch, P., He, A.W., Myers, V., Kim, M.J., Du, M., et al.: Bridgedata v2: A dataset for robot learning at scale. In: *Conference on Robot Learning*. pp. 1723–1736. PMLR (2023) **2**, **14**
 52. Wang, Y., Ding, P., Li, L., Cui, C., Ge, Z., Tong, X., Song, W., Zhao, H., Zhao, W., Hou, P., Huang, S., Tang, Y., Wang, W., Zhang, R., Liu, J., Wang, D.: Vla-adapt: An effective paradigm for tiny-scale vision-language-action model. *arXiv preprint arXiv:2509.09372* (2025) **1**, **9**, **11**, **25**, **26**
 53. Wang, Y., Yue, Z., Zeng, H., Wang, D., McAuley, J.: Train once, deploy anywhere: Matryoshka representation learning for multimodal recommendation. In: *Findings of the Association for Computational Linguistics: EMNLP 2024*. pp. 13461–13472 (2024) **14**
 54. Wu, K., Hou, C., Liu, J., Che, Z., Ju, X., Yang, Z., Li, M., Zhao, Y., Xu, Z., Yang, G., et al.: Robomind: Benchmark on multi-embodiment intelligence normative data for robot manipulation. *arXiv preprint arXiv:2412.13877* (2024) **14**
 55. Xiang, F., Qin, Y., Mo, K., Xia, Y., Zhu, H., Liu, F., Liu, M., Jiang, H., Yuan, Y., Wang, H., Yi, L., Chang, A.X., Guibas, L.J., Su, H.: SAPIEN: A simulated part-based interactive environment. In: *The IEEE Conference on Computer Vision and Pattern Recognition (CVPR)* (June 2020) **2**, **5**
 56. Yakefu, A., Xie, B., Xu, C., Zhang, E., Zhou, E., Jia, F., Yang, H., Fan, H., Zhang, H., Peng, H., et al.: Robochallenge: Large-scale real-robot evaluation of embodied policies. *arXiv preprint arXiv:2510.17950* (2025) **14**
 57. Ye, J., Gong, S., Gao, J., Fan, J., Wu, S., Bi, W., Bai, H., Shang, L., Kong, L.: Dream-vl & dream-vla: Open vision-language and vision-language-action models with diffusion language model backbone. *arXiv preprint arXiv:2512.22615* (2025) **3**
 58. Yu, T., Quillen, D., He, Z., Julian, R., Hausman, K., Finn, C., Levine, S.: Meta-world: A benchmark and evaluation for multi-task and meta reinforcement learning. In: *Conference on robot learning*. pp. 1094–1100. PMLR (2020) **14**

59. Zhang, J., Wang, K., Xu, R., Zhou, G., Hong, Y., Fang, X., Wu, Q., Zhang, Z., Wang, H.: Navid: Video-based vlm plans the next step for vision-and-language navigation. arXiv preprint arXiv:2402.15852 (2024) [13](#)
60. Zhang, S., Xu, Z., Liu, P., Yu, X., Li, Y., Gao, Q., Fei, Z., Yin, Z., Wu, Z., Jiang, Y.G., et al.: Vlabench: A large-scale benchmark for language-conditioned robotics manipulation with long-horizon reasoning tasks. In: Proceedings of the IEEE/CVF International Conference on Computer Vision. pp. 11142–11152 (2025) [14](#)
61. Zhang, W., Liu, H., Qi, Z., Wang, Y., Yu, X., Zhang, J., Dong, R., He, J., Lu, F., Wang, H., et al.: Dreamvla: a vision-language-action model dreamed with comprehensive world knowledge. arXiv preprint arXiv:2507.04447 (2025) [3](#), [7](#), [14](#)
62. Zhang, Y., Wang, R., Chen, X.: Dynamic behavior cloning with temporal feature prediction: Enhancing robotic arm manipulation in moving object tasks. IEEE Robotics and Automation Letters (2025) [14](#)
63. Zhao, T., Kumar, V., Levine, S., Finn, C.: Learning fine-grained bimanual manipulation with low-cost hardware. Robotics: Science and Systems XIX (2023) [3](#), [6](#), [9](#), [28](#), [29](#), [30](#), [31](#)
64. Zheng, R., Liang, Y., Huang, S., Gao, J., Daumé III, H., Kolobov, A., Huang, F., Yang, J.: Tracevla: Visual trace prompting enhances spatial-temporal awareness for generalist robotic policies. arXiv preprint arXiv:2412.10345 (2024) [13](#)
65. Zhu, Y., Wong, J., Mandlekar, A., Martín-Martín, R., Joshi, A., Lin, K., Madhukuri, A., Nasiriany, S., Zhu, Y.: robosuite: A modular simulation framework and benchmark for robot learning. arXiv preprint arXiv:2009.12293 (2020) [14](#)
66. Zitkovich, B., Yu, T., Xu, S., Xu, P., Xiao, T., Xia, F., Wu, J., Wohlhart, P., Welker, S., Wahid, A., et al.: Rt-2: Vision-language-action models transfer web knowledge to robotic control. In: Conference on Robot Learning. pp. 2165–2183. PMLR (2023) [13](#)

Towards Generalizable Robotic Manipulation in Dynamic Environments

Supplementary Material

This is the supplementary material for the paper "Towards Generalizable Robotic Manipulation in Dynamic Environments". We organize the content as follows:

- A** – Datasets and Implementation Details
- B** – Qualitative Results and Visualizations
- C** – Additional Methodology Description
- D** – Additional Quantitative Experiments

Level 1: Predictable Low-Order Dynamics

Drop the soft doughy bread into the medium oval breadbasket.	Use the compact stamping seal to mark Tan.	Lift the box with cards inside and shift it outward.	Grab the medium yellow cylindrical bottle, placing it into the plastic dustbin.
--	--	--	---

Level 2: Predictable High-Order Dynamics

Press the center top of the compact bell with round base.	Take the golden bread and place it inside the black pan with curved edges.	Hold the teal microphone and pass it to the other hand.	Lift the brown can, place it in the plastic basket, and raise the plastic basket.
---	--	---	---

Level 3: Stochastic and Abrupt Dynamics

Lift the paymentsign and rotate it until the QR code faces you.	Place the off-white fan on the Coral mat and verify it is facing the robot.	Use both arms to grip the medium-sized roller tightly.	Pick the barcode scanner, grab the tea box, and scan it with the barcode scanner.
---	---	--	---

Fig. 6: Qualitative demonstrations on the DOMINO dataset across hierarchical dynamic complexities. The first two columns illustrate expert trajectories in the clean setting, while the last two columns present those under domain randomization. Brief task descriptions are provided below each sequence. **Best viewed in Adobe Acrobat Reader. Animations play automatically or upon clicking.**

A Datasets and Implementation Details

A.1 Datasets

DOMINO comprises 117,000 expert trajectories covering 35 dynamic tasks across five robot embodiments. Each trajectory captures synchronized multi-view RGB observations from head and wrist cameras, alongside proprioceptive states including joint positions and end-effector poses. We apply domain randomization to enhance policy generalization. Full list of 35 dynamic tasks is in Tab. 6.

Table 6: The full list of 35 dynamic manipulation tasks in DOMINO, categorized by dynamic task type.

Dynamic Interception		
Adjust Bottle	Dump Bin Bigbin	Grab Roller
Handover Block	Handover Mic	Hanging Mug
Move Can Pot	Move Playing Card Away	Place A2B Left
Place A2B Right	Place Bread Skillet	Place Can Basket
Place Object Basket	Put Bottles Dustbin	Put Object Cabinet
Rotate QRcode	Scan Object	Shake Bottle
Shake Bottle Horizontally		
Dynamic Tracking		
Beat Block Hammer	Click Alarmclock	Click Bell
Move Pillbottle Pad	Move Stapler Pad	Place Bread Basket
Place Container Plate	Place Empty Cup	Place Fan
Place Mouse Pad	Place Object Scale	Place Object Stand
Place Phone Stand	Place Shoe	Press Stapler
Stamp Seal		

Data Storage Format. During data collection, per-frame observations are initially stored as individual pickle files before being merged into per-episode HDF5 files. Each HDF5 file contains JPEG-encoded multi-view RGB images, dual-arm and gripper joint actions, end-effector poses, and optional depth maps and point clouds. To facilitate integration with various policy learning frameworks, we provide scripts to convert the raw HDF5 data into widely used formats, such as the ALOHA HDF5 and LeRobot dataset formats. Users can also extend the pipeline to export data into custom formats.

Static Counterpart. To establish a rigorous comparison between static and dynamic manipulation capabilities, we adopt the corresponding static tasks from RoboTwin 2.0 [10]. This paired design ensures identical object models and task configurations, effectively isolating the performance impact of dynamics.

A.2 Implementation Details

Training Details. All baseline models are trained on the proposed DOMINO dataset using their official default configurations. All experiments are conducted on NVIDIA A100 GPUs. For the Qwen3-VL [1] based VLA models, the policy is initialized from Qwen3-VL-4B. The visual-language backbone hidden dimension

is 2560. The action head is implemented as an MLP and predicts 14-dimensional absolute joint actions with a future action window of 15 steps. Training uses the primary observation stream without additional proprioceptive state input, and visual observations are resized to 224×224 . The models are optimized using AdamW [33] with $\beta_1 = 0.9$, $\beta_2 = 0.95$, $\epsilon = 10^{-8}$, and weight decay 10^{-8} . We use a cosine learning rate scheduler with a linear warmup over the first 5,000 steps and a minimum learning rate of 5×10^{-7} . The learning rates for the visual-language backbone and the action head are set to 10^{-5} and 10^{-4} , respectively. The training process spans 100 epochs with a maximum of 100,000 steps. Mixed precision training and gradient checkpointing are enabled. Full-parameter fine-tuning is conducted with the DeepSpeed ZeRO-2 strategy. Training uses 8 GPUs with a per-device batch size of 8.

For the proposed PUMA, we introduce hyperparameters to effectively model the dynamic world representations and historical flow. Specifically, we employ 4 world queries and assign a weight of 0.05 to the world model loss. The world branch adopts per-frame cosine supervision on future object-centric features extracted by a frozen DINOv2-B/14 encoder. We expand both the history and future windows to 4 frames with a stride of 4. Historical observations are represented by optical flow. The resolution for historical images and optical flow computation is set to 64×64 .

Evaluation Details. We conduct closed-loop evaluations to assess the policy performance. For each task, the policy is evaluated over 100 episodes. In dynamic environments, object motion is dynamically initialized at the beginning of each episode. To simulate realistic physical interactions, the environment continuously monitors contacts between the gripper and dynamic objects. Once a contact is detected, the object stops its autonomous motion to reflect the grasping state. We enforce strict boundary checks where an episode is immediately terminated and recorded as a failure if a dynamic object moves out of the camera view. For specific tasks like lifting, success requires the vertical position of the target object to exceed a predefined threshold. In addition to the overall success rate, we track metrics including manipulation score and route completion. We also penalize erratic behaviors to thoroughly assess the robustness of the policy in dynamic environments. For the Level 1/2/3 dynamic complexity experiment in the main paper (Fig. 4), the five selected tasks are *Adjust Bottle*, *Handover Mic*, *Hanging Mug*, *Move Can Pot*, and *Place Container Plate*.

B Qualitative Results and Visualizations

We provide qualitative visualizations of the DOMINO dataset in Fig. 6. As discussed in the main paper, DOMINO is designed to evaluate robotic manipulation in dynamic environments. We build this dataset using a two-stage spatiotemporal synchronization method to collect high-quality expert demonstrations. Figures show diverse manipulation tasks across different hierarchical dynamic complexities. These tasks include both dynamic interception and dynamic tracking.

C Additional Methodology Description

This section provides supplementary details on two core components of PUMA: the optical flow computation pipeline (§C.1) and the Grounded-SAM [46] configuration for object-centric supervision (§C.2).

C.1 Optical Flow Computation

We encode scene-centric historical dynamics using optical flow maps rather than raw frames. We detail the flow computation procedure and the caching strategy designed to minimize computational overhead during training and inference.

Flow Computation. Given h sampled historical frames and the current frame, we construct h frame pairs. Both frames in each pair are first downsampled and converted to grayscale. We then compute dense optical flow using the Farneback algorithm [17]. The resulting two-channel flow field (horizontal and vertical displacements) is mapped to an HSV color space, where hue encodes motion direction and value represents motion magnitude. This HSV image is subsequently converted to RGB format to serve as the flow map input for the visual encoder. To enhance robustness, we apply percentile-based normalization to the flow magnitude, preventing occasional large motions from dominating the representation. If the magnitude falls below a predefined threshold, the flow map is zeroed out to suppress noise.

Caching Strategy. Computing optical flow on-the-fly during training introduces significant overhead. To mitigate this, we employ a disk-based caching mechanism. Each flow map is uniquely identified by a hash key encoding the dataset path, trajectory ID, step index, frame offsets, camera view, and target resolution. During the first training epoch, the computed RGB flow maps are saved as compressed NumPy arrays. In subsequent epochs, these cached maps are loaded directly, effectively amortizing the computational cost across the training process. During inference, optical flow is computed in real time. The system maintains a buffer of historical observations. At each step, the current and buffered frames are paired to compute the flow maps, which are then resized and fed into the model alongside the multi-view observations.

C.2 Grounded-SAM Configuration

We utilize a frozen grounding module to extract object-centric supervisions for auxiliary future predictor. We detail its configuration and implementation.

Module Setup. The grounding pipeline comprises two frozen models. GroundingDINO [31] uses a Swin-T backbone for open-vocabulary object detection. SAM2 [44] uses a Hiera-Large backbone for mask prediction. GroundingDINO takes an image and a text prompt as input and outputs bounding boxes with confidence scores. We filter these bounding boxes using a box threshold of 0.35 and

a text threshold of 0.25. The box with the highest score is then fed into SAM2 to generate a binary segmentation mask. Both models remain frozen during training and introduce no additional learnable parameters. We employ a rule-based parser to extract the specific target object from the language instruction as the text prompt for GroundingDINO. If this extraction fails, the complete instruction serves as the fallback prompt. This strategy ensures the grounding module focuses precisely on the manipulated objects.

Caching Strategy. Similar to the optical flow pipeline, we employ a disk-based caching mechanism for the grounding masks. Each mask is indexed by a hash comprising the model configuration, frame identity, and text prompt. Masks are computed and cached once during the initial training phase, ensuring that subsequent epochs only require disk read operations, thereby minimizing computational overhead.

D Additional Quantitative Experiments

The main paper reports the average performance metrics across all 35 tasks. This section presents the complete evaluation results for each individual task. We provide two additional sets of experimental results. Tab. 7 shows the detailed performance comparison between our approach and all baseline methods on 35 dynamic tasks. We also include comprehensive data for four transfer evaluation settings. Tab. 8, Tab. 9, Tab. 10, and Tab. 11 detail the full results for the static-to-static, static-to-dynamic, dynamic-to-static, and dynamic-to-dynamic scenarios respectively.

Table 7: Detailed per-task performance comparison of each SOTA model on the DOMINO dataset.

Task	RDT-1 [32]		OpenVLA [25]		OpenVLA-OFT [24]	
	SR↑	MS↑	SR↑	MS↑	SR↑	MS↑
<i>Adjust Bottle</i>	18.00	23.32	0.00	1.73	58.00	63.57
<i>Beat Block Hammer</i>	15.00	25.08	0.00	4.23	11.00	23.20
<i>Click Alarmclock</i>	10.00	13.55	4.00	6.02	6.00	10.53
<i>Click Bell</i>	0.00	6.07	1.00	3.29	3.00	11.24
<i>Dump Bin Bigbin</i>	0.00	10.96	0.00	2.43	0.00	17.84
<i>Grab Roller</i>	12.00	27.27	0.00	3.21	28.00	43.87
<i>Handover Block</i>	2.00	26.99	0.00	7.02	9.00	61.17
<i>Handover Mic</i>	8.00	15.16	0.00	2.34	25.00	37.58
<i>Hanging Mug</i>	7.00	18.32	0.00	3.58	12.00	35.49
<i>Move Can Pot</i>	7.00	40.88	0.00	6.80	29.00	57.26
<i>Move Pillbottle Pad</i>	0.00	9.69	0.00	1.86	1.00	9.93
<i>Move P.Card Away</i>	1.00	9.82	0.00	3.26	1.00	7.94
<i>Move Stapler Pad</i>	0.00	11.33	0.00	3.54	0.00	10.87
<i>Place A2B Left</i>	0.00	22.92	0.00	3.10	1.00	22.37
<i>Place A2B Right</i>	0.00	21.27	1.00	6.14	1.00	25.00

Continued on next page

Table 7 – Continued from previous page

Task	RDT-1 [32]		OpenVLA [25]		OpenVLA-OFT [24]	
	SR↑	MS↑	SR↑	MS↑	SR↑	MS↑
<i>Place Bread Basket</i>	2.00	8.77	0.00	4.45	1.00	7.98
<i>Place Bread Skillet</i>	4.00	15.20	0.00	7.31	1.00	20.32
<i>Place Can Basket</i>	10.00	30.84	0.00	12.21	5.00	37.78
<i>Place Container Plate</i>	1.00	12.90	0.00	4.70	10.00	16.87
<i>Place Empty Cup</i>	2.00	7.96	0.00	2.98	0.00	7.74
<i>Place Fan</i>	1.00	8.62	0.00	6.04	1.00	6.25
<i>Place Mouse Pad</i>	0.00	10.20	0.00	3.08	1.00	13.61
<i>Place Object Basket</i>	11.00	25.20	0.00	6.88	18.00	37.36
<i>Place Object Scale</i>	1.00	13.07	0.00	3.92	0.00	10.92
<i>Place Object Stand</i>	0.00	7.91	0.00	7.55	0.00	8.53
<i>Place Phone Stand</i>	1.00	13.11	0.00	3.16	0.00	12.66
<i>Place Shoe</i>	5.00	22.66	0.00	4.45	4.00	17.39
<i>Press Stapler</i>	11.00	17.30	25.00	27.12	5.00	13.53
<i>Put Bottles Dustbin</i>	12.00	21.39	1.00	7.25	19.00	29.81
<i>Put Object Cabinet</i>	12.00	36.39	0.00	6.54	1.00	42.07
<i>Rotate QRcode</i>	4.00	12.05	0.00	3.67	11.00	23.31
<i>Scan Object</i>	0.00	14.08	0.00	9.69	4.00	19.93
<i>Shake Bottle</i>	15.00	21.38	14.00	18.49	17.00	23.83
<i>Shake Bottle Horiz.</i>	14.00	24.18	8.00	12.33	31.00	38.75
<i>Stamp Seal</i>	1.00	13.93	0.00	3.13	3.00	15.47
Average	5.34	17.71	1.54	6.10	9.06	24.06
Task	π_0 -FAST [40]		VLA-Adapter [52]		InternVLA-M1 [12]	
	SR↑	MS↑	SR↑	MS↑	SR↑	MS↑
<i>Adjust Bottle</i>	11.00	37.09	9.00	38.07	20.00	62.02
<i>Beat Block Hammer</i>	1.00	18.13	1.00	15.71	0.00	17.18
<i>Click Alarmclock</i>	4.00	10.63	10.00	17.00	9.00	17.12
<i>Click Bell</i>	0.00	9.32	1.00	11.56	2.00	15.30
<i>Dump Bin Bigbin</i>	0.00	13.37	0.00	23.93	0.00	30.52
<i>Grab Roller</i>	0.00	15.59	30.00	59.19	33.00	60.47
<i>Handover Block</i>	0.00	25.35	1.00	54.15	0.00	38.71
<i>Handover Mic</i>	0.00	21.61	0.00	19.06	2.00	33.10
<i>Hanging Mug</i>	0.00	13.39	0.00	30.31	0.00	28.51
<i>Move Can Pot</i>	9.00	49.88	0.00	24.25	0.00	26.55
<i>Move Pillbottle Pad</i>	6.00	19.19	0.00	13.24	0.00	15.41
<i>Move P.Card Away</i>	0.00	20.00	0.00	22.26	0.00	24.19
<i>Move Stapler Pad</i>	0.00	17.12	0.00	13.46	0.00	14.33
<i>Place A2B Left</i>	1.00	28.69	0.00	23.02	0.00	25.63
<i>Place A2B Right</i>	0.00	27.23	0.00	22.11	0.00	27.24
<i>Place Bread Basket</i>	2.00	17.95	1.00	15.04	0.00	13.30
<i>Place Bread Skillet</i>	0.00	13.39	13.00	35.87	12.00	35.34
<i>Place Can Basket</i>	0.00	24.49	0.00	21.33	0.00	21.14
<i>Place Container Plate</i>	26.00	35.47	0.00	7.50	1.00	16.56
<i>Place Empty Cup</i>	2.00	12.11	0.00	8.41	0.00	14.37
<i>Place Fan</i>	0.00	10.93	0.00	15.14	0.00	12.14
<i>Place Mouse Pad</i>	0.00	18.23	0.00	13.74	0.00	15.15
<i>Place Object Basket</i>	0.00	25.51	0.00	23.10	1.00	26.16
<i>Place Object Scale</i>	0.00	15.18	0.00	14.31	0.00	14.61
<i>Place Object Stand</i>	2.00	11.97	0.00	12.40	0.00	17.41
<i>Place Phone Stand</i>	0.00	19.25	1.00	14.46	0.00	16.26
<i>Place Shoe</i>	3.00	16.13	0.00	12.53	0.00	17.87
<i>Press Stapler</i>	7.00	16.30	20.00	29.49	17.00	28.98
<i>Put Bottles Dustbin</i>	3.00	18.76	16.00	34.84	18.00	39.65

Continued on next page

Table 7 – Continued from previous page

Task	π_0 -FAST [40]		VLA-Adapter [52]		InternVLA-M1 [12]	
	SR \uparrow	MS \uparrow	SR \uparrow	MS \uparrow	SR \uparrow	MS \uparrow
<i>Put Object Cabinet</i>	1.00	24.13	2.00	38.14	7.00	47.28
<i>Rotate QRcode</i>	0.00	16.75	0.00	19.19	0.00	25.05
<i>Scan Object</i>	0.00	13.77	0.00	27.82	0.00	33.85
<i>Shake Bottle</i>	18.00	30.88	27.00	51.16	39.00	58.41
<i>Shake Bottle Horiz.</i>	26.00	41.11	23.00	51.98	28.00	56.48
<i>Stamp Seal</i>	2.00	21.38	0.00	17.10	0.00	18.82
Average	3.54	20.87	4.40	24.31	5.40	27.57
Task	π_0 [5]		$\pi_{0.5}$ [4]		OpenVLA-OFT*	
	SR \uparrow	MS \uparrow	SR \uparrow	MS \uparrow	SR \uparrow	MS \uparrow
<i>Adjust Bottle</i>	19.00	46.89	52.00	71.45	44.00	67.64
<i>Beat Block Hammer</i>	10.00	23.30	10.00	23.22	9.00	22.47
<i>Click Alarmclock</i>	15.00	18.95	14.00	18.47	5.00	10.07
<i>Click Bell</i>	0.00	8.04	0.00	6.35	1.00	11.56
<i>Dump Bin Bigbin</i>	0.00	20.88	0.00	16.64	0.00	29.44
<i>Grab Roller</i>	11.00	31.46	10.00	34.32	31.00	53.45
<i>Handover Block</i>	0.00	39.21	1.00	33.95	0.00	44.75
<i>Handover Mic</i>	4.00	26.18	5.00	29.10	21.00	50.93
<i>Hanging Mug</i>	9.00	26.03	5.00	25.59	0.00	28.51
<i>Move Can Pot</i>	16.00	41.72	7.00	40.34	13.00	37.07
<i>Move Pillbottle Pad</i>	7.00	16.53	6.00	15.93	7.00	15.81
<i>Move P.Card Away</i>	7.00	21.53	8.00	24.84	0.00	27.98
<i>Move Stapler Pad</i>	1.00	11.96	0.00	13.38	0.00	14.18
<i>Place A2B Left</i>	2.00	21.81	2.00	26.04	1.00	34.14
<i>Place A2B Right</i>	1.00	20.08	1.00	23.63	4.00	33.38
<i>Place Bread Basket</i>	6.00	11.67	8.00	15.89	7.00	22.30
<i>Place Bread Skillet</i>	2.00	16.11	9.00	22.30	19.00	38.30
<i>Place Can Basket</i>	8.00	37.49	6.00	29.48	0.00	29.17
<i>Place Container Plate</i>	15.00	21.79	22.00	28.46	8.00	17.02
<i>Place Empty Cup</i>	0.00	8.05	2.00	12.71	1.00	11.59
<i>Place Fan</i>	2.00	9.91	2.00	11.72	0.00	6.54
<i>Place Mouse Pad</i>	4.00	14.93	5.00	19.03	1.00	17.29
<i>Place Object Basket</i>	16.00	33.55	11.00	30.19	6.00	35.01
<i>Place Object Scale</i>	0.00	9.71	3.00	15.37	0.00	15.06
<i>Place Object Stand</i>	1.00	8.00	1.00	8.97	1.00	13.68
<i>Place Phone Stand</i>	0.00	13.11	2.00	17.98	0.00	17.86
<i>Place Shoe</i>	20.00	32.11	25.00	32.84	6.00	19.36
<i>Press Stapler</i>	9.00	18.77	6.00	13.27	9.00	17.64
<i>Put Bottles Dustbin</i>	20.00	37.01	17.00	33.30	43.00	56.41
<i>Put Object Cabinet</i>	11.00	41.38	11.00	46.24	26.00	59.78
<i>Rotate QRcode</i>	6.00	15.90	4.00	17.90	3.00	25.08
<i>Scan Object</i>	0.00	19.64	1.00	20.48	4.00	31.66
<i>Shake Bottle</i>	28.00	44.02	33.00	49.40	53.00	67.42
<i>Shake Bottle Horiz.</i>	33.00	53.03	42.00	62.72	52.00	65.78
<i>Stamp Seal</i>	3.00	17.75	6.00	22.58	5.00	18.69
Average	8.17	23.96	9.63	26.17	10.90	30.49
Task	Isaac-GROOT*		π_0 -FAST*		PUMA(OURS)	
	SR \uparrow	MS \uparrow	SR \uparrow	MS \uparrow	SR \uparrow	MS \uparrow
<i>Adjust Bottle</i>	19.00	50.82	8.00	33.15	65.00	74.04
<i>Beat Block Hammer</i>	3.00	21.53	4.00	17.87	15.00	29.09
<i>Click Alarmclock</i>	11.00	18.50	18.00	20.75	4.00	8.38
<i>Click Bell</i>	2.00	14.82	1.00	7.62	3.00	13.64

Continued on next page

Table 7 – Continued from previous page

Task	Isaac-GR00T*		π_0 -FAST*		PUMA(OURS)	
	SR \uparrow	MS \uparrow	SR \uparrow	MS \uparrow	SR \uparrow	MS \uparrow
<i>Dump Bin Bigbin</i>	0.00	26.91	0.00	12.91	0.00	39.05
<i>Grab Roller</i>	28.00	53.56	20.00	46.32	33.00	56.48
<i>Handover Block</i>	0.00	44.88	2.00	31.34	17.00	64.79
<i>Handover Mic</i>	3.00	35.52	5.00	23.84	35.00	54.40
<i>Hanging Mug</i>	0.00	32.21	1.00	20.06	9.00	41.74
<i>Move Can Pot</i>	1.00	35.09	9.00	35.02	22.00	47.80
<i>Move Pillbottle Pad</i>	0.00	12.94	1.00	9.67	14.00	21.82
<i>Move P.Card Away</i>	0.00	25.95	6.00	29.73	6.00	27.90
<i>Move Stapler Pad</i>	0.00	15.97	0.00	12.71	1.00	16.24
<i>Place A2B Left</i>	0.00	27.02	3.00	25.02	13.00	41.65
<i>Place A2B Right</i>	0.00	26.63	1.00	23.83	8.00	34.39
<i>Place Bread Basket</i>	1.00	18.65	0.00	12.53	12.00	22.44
<i>Place Bread Skillet</i>	10.00	30.34	2.00	26.15	19.00	35.95
<i>Place Can Basket</i>	0.00	30.30	0.00	22.91	14.00	45.79
<i>Place Container Plate</i>	4.00	19.55	7.00	16.85	26.00	34.45
<i>Place Empty Cup</i>	0.00	15.68	0.00	8.99	7.00	17.85
<i>Place Fan</i>	2.00	11.88	1.00	6.87	8.00	14.36
<i>Place Mouse Pad</i>	0.00	17.91	0.00	14.04	2.00	17.86
<i>Place Object Basket</i>	1.00	31.11	7.00	21.74	13.00	41.67
<i>Place Object Scale</i>	0.00	16.87	2.00	13.50	4.00	16.05
<i>Place Object Stand</i>	1.00	17.65	0.00	10.25	1.00	10.66
<i>Place Phone Stand</i>	0.00	18.84	1.00	15.28	6.00	19.02
<i>Place Shoe</i>	0.00	17.21	9.00	19.82	16.00	27.23
<i>Press Stapler</i>	9.00	22.64	25.00	32.76	10.00	18.40
<i>Put Bottles Dustbin</i>	13.00	33.42	3.00	20.39	23.00	36.82
<i>Put Object Cabinet</i>	14.00	50.22	2.00	13.11	34.00	61.64
<i>Rotate QRcode</i>	0.00	28.08	0.00	11.72	14.00	29.27
<i>Scan Object</i>	3.00	30.69	0.00	20.21	5.00	30.58
<i>Shake Bottle</i>	43.00	60.65	28.00	33.48	55.00	65.37
<i>Shake Bottle Horiz.</i>	46.00	67.33	34.00	39.33	75.00	80.57
<i>Stamp Seal</i>	0.00	19.65	1.00	13.23	13.00	26.50
Average	6.10	28.60	5.74	20.66	17.20	34.97

* Indicates that the method is implemented using Qwen3-VL [11].

Table 8: Detailed quantitative evaluation of VLA models in the static setting ($S \rightarrow S$). This table reports the per-task performance across all 35 tasks for models trained and evaluated in the static environment. These results expand upon the *Static* columns in Tab. 1 of the main text.

Simulation Task	ACT [63]		OpenVLA-OFT [24]		$\pi_{0.5}$ [4]	
	SR	MS	SR	MS	SR	MS
<i>Adjust Bottle</i>	97%	97.00	47%	47.00	92%	92.00
<i>Beat Block Hammer</i>	53%	53.00	12%	12.00	55%	55.00
<i>Click Alarmclock</i>	29%	29.00	57%	57.00	48%	48.00
<i>Click Bell</i>	59%	59.00	24%	24.00	58%	58.00
<i>Dump Bin Bigbin</i>	66%	66.00	18%	18.00	73%	73.00
<i>Grab Roller</i>	95%	95.00	47%	47.00	98%	98.00
<i>Handover Block</i>	43%	43.00	3%	3.00	2%	2.00
<i>Handover Mic</i>	82.00	82.00	93%	93.00	63%	63.00
<i>Hanging Mug</i>	13%	13.00	1%	1.00	3%	3.00
<i>Move Can Pot</i>	23%	23.00	34%	34.00	14%	14.00
<i>Move Pillbottle Pad</i>	1%	1.00	1%	1.00	20%	20.00
<i>Move P.Card Away</i>	34%	34.00	6%	6.00	74%	74.00
<i>Move Stapler Pad</i>	0%	0.00	0%	0.00	8%	8.00
<i>Place A2B Left</i>	0%	0.00	2%	2.00	39%	39.00
<i>Place A2B Right</i>	0%	0.00	0%	0.00	38%	38.00
<i>Place Bread Basket</i>	4%	4.00	6%	6.00	42%	42.00
<i>Place Bread Skillet</i>	9%	9.00	4%	4.00	39%	39.00
<i>Place Can Basket</i>	1%	1.00	8%	8.00	17%	17.00
<i>Place Container Plate</i>	72%	72.00	27%	27.00	90%	90.00
<i>Place Empty Cup</i>	58%	58.00	1%	1.00	68%	68.00
<i>Place Fan</i>	0%	0.00	3%	3.00	30%	30.00
<i>Place Mouse Pad</i>	0%	0.00	0%	0.00	22%	22.00
<i>Place Object Basket</i>	18%	18.00	19%	19.00	57%	57.00
<i>Place Object Scale</i>	0%	0.00	0%	0.00	41%	41.00
<i>Place Object Stand</i>	0%	0.00	17%	17.00	57%	57.00
<i>Place Phone Stand</i>	1%	1.00	3%	3.00	37%	37.00
<i>Place Shoe</i>	3%	3.00	3%	3.00	39%	39.00
<i>Press Stapler</i>	31%	31.00	35%	35.00	35%	35.00
<i>Put Bottles Dustbin</i>	28%	28.00	1%	1.00	10%	10.00
<i>Put Object Cabinet</i>	9%	9.00	11%	11.00	36%	36.00
<i>Rotate QRcode</i>	3%	3.00	10%	10.00	54%	54.00
<i>Scan Object</i>	1%	1.00	0%	0.00	7%	7.00
<i>Shake Bottle</i>	74%	74.00	63%	63.00	95%	95.00
<i>Shake Bottle Horiz.</i>	63%	63.00	57%	57.00	97%	97.00
<i>Stamp Seal</i>	1%	1.00	0%	0.00	11%	11.00
Average (%)	27.74	27.74	17.51	17.51	44.83	44.83

Table 9: Detailed quantitative evaluation of VLA models in the zero-shot dynamic setting ($S \rightarrow D$). This table reports the per-task performance across all 35 tasks for models trained in a static environment and directly evaluated in our proposed DOMINO without fine-tuning. These results expand upon the *ZS* columns in Tab. 1 of the main text.

Simulation Task	ACT [63]		OpenVLA-OFT [24]		$\pi_{0.5}$ [4]	
	SR	MS	SR	MS	SR	MS
<i>Adjust Bottle</i>	37%	46.18	16%	26.19	12%	24.65
<i>Beat Block Hammer</i>	17%	30.85	7%	19.99	23%	36.32
<i>Click Alarmclock</i>	3%	5.80	9%	13.63	8%	13.92
<i>Click Bell</i>	0%	7.89	1%	9.41	1%	10.77
<i>Dump Bin Bigbin</i>	0%	15.42	0%	14.31	0%	15.70
<i>Grab Roller</i>	24%	52.27	24%	39.02	6%	20.18
<i>Handover Block</i>	0%	49.51	3%	29.02	0%	29.13
<i>Handover Mic</i>	13%	36.52	8%	18.30	7%	7.00
<i>Hanging Mug</i>	21%	36.38	11%	23.98	0%	13.82
<i>Move Can Pot</i>	0%	42.52	29%	49.75	5%	37.66
<i>Move Pillbottle Pad</i>	0%	14.99	0%	11.24	5%	16.76
<i>Move P. Card Away</i>	9%	32.83	0%	13.92	1%	15.87
<i>Move Stapler Pad</i>	0%	19.83	0%	10.46	2%	13.90
<i>Place A2B Left</i>	0%	27.15	3%	23.52	3%	24.65
<i>Place A2B Right</i>	0%	28.01	0%	17.74	1%	22.73
<i>Place Bread Basket</i>	0%	16.71	0%	15.94	17%	22.80
<i>Place Bread Skillet</i>	5%	33.74	1%	17.92	5%	15.43
<i>Place Can Basket</i>	1%	32.08	8%	37.73	7%	23.75
<i>Place Container Plate</i>	24%	30.77	14%	20.61	33%	38.11
<i>Place Empty Cup</i>	2%	11.59	0%	7.46	7%	13.74
<i>Place Fan</i>	0%	10.97	0%	4.57	1%	10.85
<i>Place Mouse Pad</i>	0%	24.06	0%	13.63	6%	18.59
<i>Place Object Basket</i>	19%	30.93	16%	35.51	6%	23.96
<i>Place Object Scale</i>	1%	17.69	0%	9.10	5%	15.93
<i>Place Object Stand</i>	0%	13.27	2%	17.23	3%	11.39
<i>Place Phone Stand</i>	0%	22.93	0%	14.73	1%	16.35
<i>Place Shoe</i>	1%	31.70	6%	21.76	28%	36.09
<i>Press Stapler</i>	2%	11.00	2%	12.31	1%	10.59
<i>Put Bottles Dustbin</i>	0%	17.39	29%	47.36	13%	28.30
<i>Put Object Cabinet</i>	7%	27.01	7%	24.61	2%	17.23
<i>Rotate QRcode</i>	0%	34.38	8%	17.51	2%	13.31
<i>Scan Object</i>	2%	25.78	0%	7.15	0%	14.22
<i>Shake Bottle</i>	18%	36.52	12%	16.43	19%	24.15
<i>Shake Bottle Horiz.</i>	23%	45.63	19%	25.61	24%	32.82
<i>Stamp Seal</i>	0%	15.73	0%	12.93	7%	24.76
Average (%)	6.54	26.74	6.71	20.02	7.46	20.44

Table 10: Detailed quantitative evaluation of VLA models transferring from dynamic to static settings ($D \rightarrow S$). This table reports the per-task performance across all 35 tasks for models trained in the dynamic environment (DOMINO) and evaluated back in the standard static environment.

Simulation Task	ACT [63]		OpenVLA-OFT [24]		$\pi_{0.5}$ [4]	
	SR	MS	SR	MS	SR	MS
<i>Adjust Bottle</i>	97%	97.00	65%	65.00	70%	70.00
<i>Beat Block Hammer</i>	0%	0.00	18%	38.42	27%	27.00
<i>Click Alarmclock</i>	7%	7.00	24%	24.00	24%	24.00
<i>Click Bell</i>	6%	6.00	10%	10.00	13%	13.00
<i>Dump Bin Bigbin</i>	20%	20.00	23%	23.00	26%	26.00
<i>Grab Roller</i>	59%	59.00	42%	42.00	59%	59.00
<i>Handover Block</i>	14%	14.00	5%	5.00	3%	3.00
<i>Handover Mic</i>	1%	1.00	0%	0.00	7%	7.00
<i>Hanging Mug</i>	6%	6.00	3%	3.00	4%	4.00
<i>Move Can Pot</i>	36%	36.00	20%	20.00	11%	11.00
<i>Move Pillbottle Pad</i>	5%	5.00	2%	2.00	7%	7.00
<i>Move P.Card Away</i>	2%	2.00	5%	5.00	26%	26.00
<i>Move Stapler Pad</i>	0%	0.00	0%	0.00	0%	0.00
<i>Place A2B Left</i>	0%	0.00	0	0.00	19%	19.00
<i>Place A2B Right</i>	0%	0.00	0%	0.00	21%	21.00
<i>Place Bread Basket</i>	0%	0.00	0%	0.00	3%	3.00
<i>Place Bread Skillet</i>	1%	1.00	0%	0.00	2%	2.00
<i>Place Can Basket</i>	3%	3.00	3%	3.00	17%	17.00
<i>Place Container Plate</i>	67%	67.00	40%	40.00	73%	73.00
<i>Place Empty Cup</i>	37%	37.00	1%	1.00	43%	43.00
<i>Place Fan</i>	0%	0.00	0%	0.00	6%	6.00
<i>Place Mouse Pad</i>	0%	0.00	0%	0.00	3%	3.00
<i>Place Object Basket</i>	19%	19.00	23%	23.00	16%	16.00
<i>Place Object Scale</i>	0%	0.00	0%	0.00	8%	8.00
<i>Place Object Stand</i>	0%	0.00	22%	22.00	27%	27.00
<i>Place Phone Stand</i>	0%	0.00	1%	1.00	20%	20.00
<i>Place Shoe</i>	0%	0.00	5%	5.00	15%	15.00
<i>Press Stapler</i>	31%	31.00	51%	51.00	35%	35.00
<i>Put Bottles Dustbin</i>	0%	0.00	0%	0.00	1%	1.00
<i>Put Object Cabinet</i>	1%	1.00	7%	7.00	20%	20.00
<i>Rotate QRcode</i>	0%	0.00	12%	12.00	10%	10.00
<i>Scan Object</i>	0%	0.00	2%	2.00	5%	5.00
<i>Shake Bottle</i>	43%	43.00	54%	54.00	83%	83.00
<i>Shake Bottle Horiz.</i>	34%	34.00	55%	55.00	84%	84.00
<i>Stamp Seal</i>	0%	0.00	0%	0.00	1%	1.00
Average (%)	13.97	13.97	14.09	14.67	22.54	22.54

Table 11: Detailed quantitative evaluation of VLA models in the fine-tuning dynamic setting ($D \rightarrow D$). This table reports the per-task success rates across all 35 tasks for models fine-tuned and evaluated in the dynamic environment. These results expand upon the *FT* columns in Tab. 1 of the main text.

Simulation Task	ACT [63]		OpenVLA-OFT [24]		$\pi_{0.5}$ [4]	
	SR	MS	SR	MS	SR	MS
<i>Adjust Bottle</i>	65%	67.57	58%	63.57	52%	71.45
<i>Beat Block Hammer</i>	0%	5.14	11%	23.20	10%	23.22
<i>Click Alarmclock</i>	8%	11.05	6%	10.53	14%	18.47
<i>Click Bell</i>	0%	8.24	3%	11.24	0%	6.35
<i>Dump Bin Bigbin</i>	0%	11.14	0%	17.84	0%	16.64
<i>Grab Roller</i>	23%	47.80	28%	43.87	10%	34.32
<i>Handover Block</i>	11%	51.07	9%	61.17	1%	33.95
<i>Handover Mic</i>	23%	40.35	25%	37.58	5%	29.10
<i>Hanging Mug</i>	28%	43.62	12%	35.49	5%	25.59
<i>Move Can Pot</i>	26%	53.55	29%	57.26	7%	40.34
<i>Move Pillbottle Pad</i>	1%	8.15	1%	9.93	6%	15.93
<i>Move P.Card Away</i>	1%	26.54	1%	7.94	8%	24.84
<i>Move Stapler Pad</i>	0%	13.12	0%	10.87	0%	13.38
<i>Place A2B Left</i>	0%	21.39	1%	22.37	2%	26.04
<i>Place A2B Right</i>	0%	28.33	1%	25.00	1%	23.63
<i>Place Bread Basket</i>	1%	15.05	1%	7.98	8%	15.89
<i>Place Bread Skillet</i>	12%	28.54	1%	20.32	9%	22.30
<i>Place Can Basket</i>	4%	29.47	5%	37.78	6%	29.48
<i>Place Container Plate</i>	30%	35.75	10%	16.87	22%	28.46
<i>Place Empty Cup</i>	6%	12.49	0%	7.74	2%	12.71
<i>Place Fan</i>	1%	6.64	1%	6.25	2%	11.72
<i>Place Mouse Pad</i>	0%	14.31	1%	13.61	5%	19.03
<i>Place Object Basket</i>	21%	35.96	18%	37.36	11%	30.19
<i>Place Object Scale</i>	0%	12.89	0%	10.92	3%	15.37
<i>Place Object Stand</i>	0%	7.42	0%	8.53	1%	8.97
<i>Place Phone Stand</i>	0%	16.45	0%	12.66	2%	17.98
<i>Place Shoe</i>	0%	7.92	4%	17.39	25%	32.84
<i>Press Stapler</i>	4%	15.31	5%	13.53	6%	13.27
<i>Put Bottles Dustbin</i>	21%	38.57	19%	29.81	17%	33.30
<i>Put Object Cabinet</i>	2%	39.61	1%	42.07	11%	46.24
<i>Rotate QRcode</i>	0%	12.63	11%	23.31	4%	17.90
<i>Scan Object</i>	2%	19.82	4%	19.93	1%	20.48
<i>Shake Bottle</i>	14%	27.23	17%	23.83	33%	49.40
<i>Shake Bottle Horiz.</i>	18%	41.70	31%	38.75	42%	62.72
<i>Stamp Seal</i>	8%	19.10	3%	15.47	6%	22.58
Average (%)	9.43	24.97	9.06	24.06	9.63	26.12